scientific reports

Check for updates

OPEN

Transforming tire-derived char into powerful arsenic adsorbents by mild modification

Yunnen Chen✉, Jiali Xu & Yuting Li

A large amount of arsenic-containing wastewater discharged by the non-ferrous metal industry will cause serious environmental problems if it is not properly treated. Pyrolysis char of waste tire is a kind of solid waste. Since the surface properties of tire derived char (TC) are affected by tar/ash adhesion during pyrolysis, it is necessary to modify TC to treat wastewater containing As(V) effectively as an adsorbent. At present, most studies on the modification of TC are prepared into activated carbon by high temperature activation in N_2 atmosphere. In this study, TC was modified at room temperature and air atmosphere, and $Fe(OH)_3$-TC_{NaOH} adsorbent with particle size of 61–75 μm was obtained under the premise of the removal rate of As(V) and the settling performance of the adsorbent. When the initial concentration of As(V) was 5 mg/L, the removal rate of As(V) by $Fe(OH)_3$-TC_{NaOH} with a particle size of 61–75 μm could reach 90% within 30 min under a wide pH range (3–9). The adsorption of As(V) by $Fe(OH)_3$-TC_{NaOH} was most affected by the coexistence of PO_4^{3-}, which resulted in the removal rate of As(V) decreased by about 20%. The adsorption mechanism shows that the significant increase in the number of 3–5 nm mesoporous pores of $Fe(OH)_3$-TC_{NaOH} and the formation of H bonds are beneficial to the adsorption of $Fe(OH)_3$-TC_{NaOH} to As(V), and improve the stability of Fe-As complex.

Keywords Waste tire pyrolysis char, Arsenic-containing wastewater, Modification treatment, Adsorption mechanism, Sedimentation performance

While the rapid development of the transportation industry has brought great convenience to people's lives, and the consumption and wear of automobile tires have also produced a mass of waste tires. In 2022, China's waste tire production was about 350 million, and its annual growth rate is 8–10% [1]. The accumulation of waste tires not only occupies a large amount of land and provides breeding places for mosquitoes, but also produces a large number of carcinogens such as polycyclic aromatic hydrocarbons due to tire fire, causing serious environmental pollution[2,3]. Recycling waste tires is the most effective way to reduce their impact on the environmental. At present, the recycling methods of waste tires mainly include prototype utilization, tire retreading[4] and various thermochemical processes (pyrolysis, incineration, direct liquefaction)[5]. Prototype utilization is to use waste tires directly in the fields such as hillside soil consolidation and ship collision prevention, but its usage is less[6,7]. Thanks to possible safety hazards, the quality of retreaded tires is difficult to get the trust of consumers[8]. Among these thermochemical processes, pyrolysis has attracted much attention due to its low secondary pollution and the production of useful industrial raw materials such as solid char, liquid hydrocarbon fuels and gases[9]. As the key pyrolysis product, char directly affects the economic benefit of waste tire pyrolysis. How to improve the utilization value of char is one of the research hotspots of waste tire pyrolysis.

The pyrolysis char of waste tire is mainly composed of carbon black added in the process of tire production, other inorganic fillers and coke deposited on the surface of char, etc. The tar, deposited carbon and ash on the surface of char cover its original active sites and reduce its specific surface area, thus limit the high-value utilization of char[10–12]. The ash content of char can be reduced from 15.0 to 4.9 wt% by pickling[13]. Physical or chemical activation processes can increase the pore volume fraction of char, thereby increasing its specific surface area and surface activity[14,15]. In the physical activation process, the carbonization degree of char is first improved at a lower temperature, and then treated with reaction gas (carbon dioxide or water vapor) at high temperature, and part of the amorphous carbon and crystalline carbon in the char are removed by gasification reaction to improve the porosity[16]. Chemical activation typically uses activators such as $ZnCl_2$, H_3PO_4, and KOH as substrates for pore development, which oxidizes at relatively low temperatures and ultimately helps to increase the specific surface area of the char[17].

Jiangxi Provincial Key Laboratory of Environmental Pollution Prevention and Control in Mining and Metallurgy, Jiangxi University of Science and Technology, No. 156 Kejia Ave, Ganzhou 341000, Jiangxi, People's Republic of China. ✉email: cyn70yellow@126.com

Excessive concentrations of arsenic in water bodies are threatening the health of billions of people worldwide[18]. Arsenic (As) and its compounds, as one of class I carcinogen listed by the World Health Organization (WHO), have become a global concern for water pollution[18]. Current treatment methods for arsenic-containing water include chemical precipitation[19], membrane method[20], biological method[21], electric flocculation[22] and adsorption[23], etc. Adsorption is a physicochemical technique that is considered one of the most effective methods because it is simple to operate, there is no secondary pollution[24]. Many materials, such as spent grain, have been developed as adsorbents to remove arsenic from waters[25]. It is feasible to remove As(V) from aqueous solution by using bone char as adsorbent[26].

At present, it is reported that waste tire pyrolysis char is used as an adsorbent to remove heavy metals such as lead, copper and zinc from wastewater[27]. The use of char to treat arsenic in wastewater has also been studied. The adsorption material obtained by mixing the hydrochloric acid pretreated char with $Al(OH)_3$ and heating at 700 °C in N_2 atmosphere has a good arsenic removal effect[28]. The adsorbent obtained by soaking char in HNO_3 and then calcination in N_2 at 350 °C has mesoporous carbon structure and adsorption capacity of As(III) was 0.8 mg/g[29]. The above studies show that whether it is to remove Pb, Cu, Zn or As from wastewater, pyrolysis char needs to be converted into activated carbon under relatively harsh conditions such as high temperature and N_2 atmosphere, which consumes a lot of energy. On the other hand, the settling performance of char adsorbent and their separation from heavy metals or arsenic are less studied.

In this study, the tar/ash on the surface of tire-derived char (TC) was first removed at room temperature and in an air atmosphere, followed by chemical activation. The efficiency of modified TC in removing As(V) from aqueous solution was evaluated. Special attention was paid to the adsorbent settling performance and the adsorption mechanisms of modified TC by characterization using pore size distributions, phase analysis, energy spectrum analysis and X-ray photoelectron spectroscopy (XPS) analyses.

Materials and methods

Experimental materials

TC was sourced from a waste tire pyrolysis plant in Jiangxi, China. It was thoroughly washed with deionized (DI) water to remove sand, placed in an oven at 70 °C for 24 h until completely dried, ground and passed through a 150 μm sieve.

Stock solutions (5 mg/L) were prepared from sodium arsenate ($Na_3AsO_4{\cdot}12H_2O$; greater than 99.0%) for As(V). The prepared stock solutions were further diluted with appropriate amounts of DI water to obtain the working experimental solutions with concentrations of 0.5, 1, 2, 3 and 4 mg/L.

HCl, HNO_3, H_2SO_4 and NaOH were used to remove the tar/ash on TC surface and for adjusting the solution pH. $Ca(OH)_2$ and $FeCl_3{\cdot}6H_2O$ were used as modifier to modify TC.

In this work, all chemicals used were analytical grade.

Modification of TC

TC was modified using a two-step sequence: tar/ash removal and chemical activation. First, TC was added into conical bottles containing 2 mol/L HCl, HNO_3, H_2SO_4, NaOH solution and saturated $Ca(OH)_2$ solution respectively (solid-liquid ratio 100 g/1 L). The conical bottles were placed in 25 °C, 150 r/min water bath thermostatic oscillator for 24 h. Then the solid material was filtered (pore size 0.45 μm), washed with DI water until the effluent pH was neutral, and dried in the oven at 70 °C for 12 h to obtain acid/alkali modified TC. They were denoted as TC_{HCl}, TC_{HNO3}, TC_{H2SO4}, TC_{NaOH} and $TC_{Ca(OH)2}$, respectively. The subsequent chemical activation step was to add TC and TC_{NaOH} into 0.1 mol/L $FeCl_3$ solution respectively (solid-liquid ratio 100 g/1 L) and stir the suspension until the mixture was uniform. Then add 1 mol/L NaOH solution drop by drop to adjust the pH of the suspension to 7.20, stir continuously for 2 h and stabilize the pH at 7.20. The solid material was filtered (pore size 0.45 μm) and washed with DI water until the effluent pH was neutral, and then dried in 70 °C oven for 12 h. The final products were denoted as $Fe(OH)_3$-TC and $Fe(OH)_3$-TC_{NaOH}, respectively.

Batch adsorption tests

(1) Determination of the best removal method of tar/ash in TC. The effect of acid/base modification on the removal rate of As(V) in TC was investigated under the conditions of initial As(V) concentration of 5 mg/L, pH of solution of 9 and dosage of adsorbent of 0.8 g/L by oscillating at 25 °C for 10 min with a water bath thermostatic oscillator. The As(V) removal performance of TC was compared under the same conditions.

(2) The effect of chemical activation on the removal of As(V) from Fe-modified TC (including $Fe(OH)_3$-TC and $Fe(OH)_3$-TC_{NaOH}) was studied by using a water bath thermostatic oscillator with an initial As(V) concentration of 5 mg/L, pH of 9, dosage 0.4–1.0 g/L, and constant temperature of 25 °C for 10 min. The As(V) removal performance of TC was compared under the same conditions.

(3) The effect of particle size on sedimentation and adsorption of As(V). $Fe(OH)_3$-TC_{NaOH} with different particle sizes were added into a colorimetric tube containing DI water at a solid-liquid ratio of 0.8 g/L to observe the precipitation effect.

(4) The effects of reaction time (5–60 min), pH value of solution (3–11), As(V) initial concentration (0.5-5 mg/L), reaction temperature (25–55 °C) and coexisting ions on the As(V) removal effect of $Fe(OH)_3$-TC_{NaOH} were investigated with the consideration of sedimentation and As(V) removal performance.

1 mol/L HCl and NaOH solution were used to adjust the solution pH to the set value.

The concentration of As(V) in the raw and treated simulation wastewater was investigated with the Inductively Coupled Plasma spectrometer (ICP).

All experimental runs in this study were repeated three times, and data obtained represented the mean values. the removal effect of TC was investigated.

Results and discussions

Effect of acid/base modified TC on adsorption of As(V)

In order to remove the tar/ash on the TC surface and improve its specific surface area and surface activity, acid and alkali were used to modify TC. The particle size of TC and various modified TC is less than 150 μm. The adsorption effect of acid/alkali modified TC (tar/ash removal) on As(V) is shown in Fig. 1.

As can be seen from Fig. 1, the removal rate of TC for As(V) was 7.4%, while the removal of TC_{HCl}, TC_{HNO3}, TC_{H2SO4}, TC_{NaOH} and $TC_{Ca(OH)2}$ for As(V) were 0, 0, 0, 46.0 and 44.6%, respectively. Obviously, the adsorption effect of acid/alkali modified char on As(V) is very different. Acid modification has an inhibitory effect on the adsorption of As(V) by TC, which may be due to the reaction of the acid with the functional group of TC surface to form a carboxylate substance that can inhibit the adsorption of As(V)[29]. However, alkali modification may remove most of the tar and ash on TC surface, thereby increasing the specific surface area of TC and improving the adsorption of As(V). Since TC_{NaOH} had a slightly better removal effect on As(V) than that of $TC_{Ca(OH)2}$, subsequent experiments were conducted on the basis of TC_{NaOH}.

In the experiment, it was also observed that at the end of the oscillatory adsorption, part of the adsorbent was still suspended in the solution for a long time, and could not completely settle to the bottom after standing for 10 min, indicating that the settling effect of some TC/modified TC was poor.

Effect of chemical activation on removal of As(V) by Fe-modified TC

Taking the amount of adsorbent as variable, the removal effect of Fe-modified TC on As(V) was investigated and compared with that of TC under the same conditions. The particle size of TC and various modified TC is less than 150 μm. The results are shown in Fig. 2.

From Fig. 2 can be seen that the removal rate of TC, $Fe(OH)_3$-TC and $Fe(OH)_3$-TC_{NaOH} for As(V) increased with the increase of adsorbent dosage. When the adsorbent dosage increased from 0.4 to 1.0 g/L, the removal rates of TC, $Fe(OH)_3$-TC and $Fe(OH)_3$-TC_{NaOH} for As(V) increased from 1.6, 29.1 and 43.0% to 15.8, 79.0 and 86.2%, respectively. This is because the increase in the amount of adsorbent actually increases the available adsorption sites, which is conducive to the adsorption of As(V) in the solution. In addition, the removal effect of $Fe(OH)_3$-TC and $Fe(OH)_3$-TC_{NaOH} on As(V) was much greater than that of TC at the four doses.

In addition, the As(V) removal rate of the three adsorbents was slightly increased when the adsorbents dosage increased from 0.8 to 1.0 g/L. Considering the cost, the dosage of subsequent adsorbent was selected to be 0.8 g/L. It can also be seen from Fig. 2 that the removal rate of $Fe(OH)_3$-TC_{NaOH} for As(V) was higher than that of $Fe(OH)_3$-TC at the four dosage levels. Therefore, $Fe(OH)_3$-TC_{NaOH} was selected for subsequent experiments.

It was also observed in the experiment that part of the adsorbent in the reaction system could not completely settle to the bottom at the end of the adsorption.

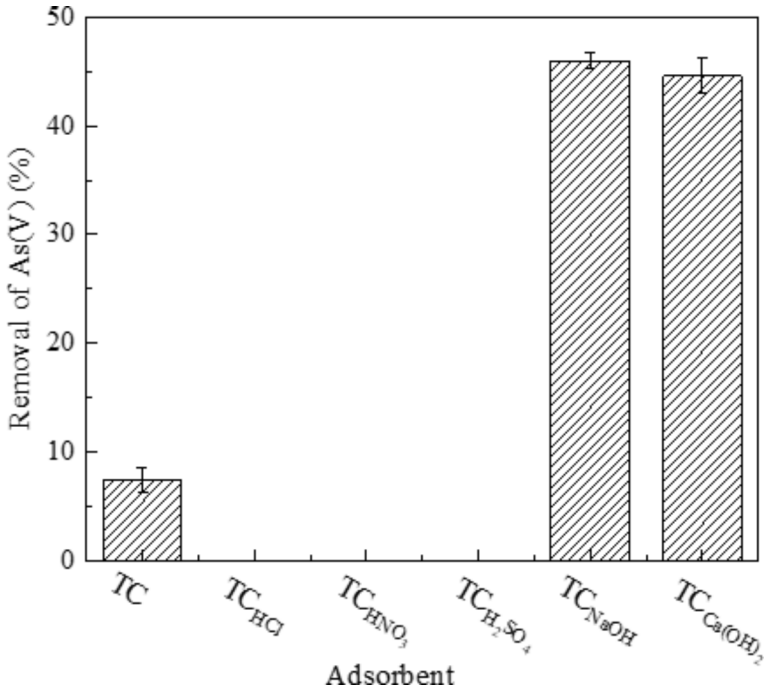

Fig. 1. Effect of acid/base modified TC on adsorption of As(V) (initial concentration of As(V) was 5 mg/L, pH in solution 9, dosage of adsorbent 0.8 g/L, reaction temperature 25 °C, reaction time 10 min).

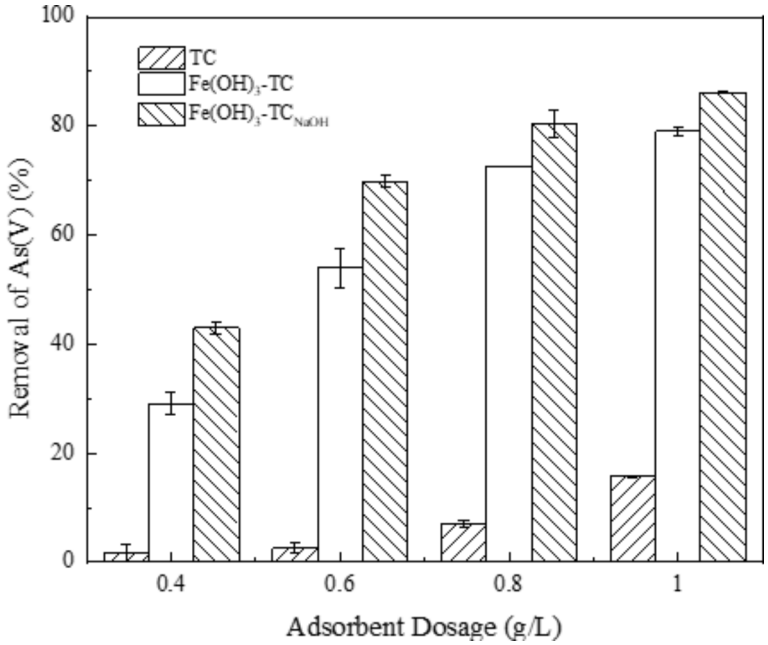

Fig. 2. Effect of adsorbent dosage on removal of As(V) from Fe-modified TC (initial concentration of As(V) was 5 mg/L, pH in solution 9, reaction temperature 25 °C, reaction time 10 min).

Effect of particle size on settling performance of $Fe(OH)_3$-TCNaOH and adsorption of As(V)

In practical applications, the sedimentation performance of adsorbent is very important. The settling effect of $Fe(OH)_3$-TC_{NaOH} with particle sizes 125–150 μm, 106–125 μm, 98–106 μm, 90–98 μm, 75–90 μm, 67–75 μm, 61–67 μm and < 61 μm are shown in Fig. 3.

As can be seen from Fig. 3, particle size plays a major role in the sedimentation process, and this result is consistent with the study of Therdkiattikul[30]. After standing for 5 min (Fig. 3(f)), only $Fe(OH)_3$-TC_{NaOH} with particle size < 61 μm still had a large number of particles suspended in water, making the suspension appear black, while $Fe(OH)_3$-TC_{NaOH} of other particle sizes basically settled completely. Note that within 5 min of standing, all particle sizes of $Fe(OH)_3$-TC_{NaOH} have a layer of black at the top of the colorimetric tube, which is a small part of light ash floating on the water.

The adsorption effect of $Fe(OH)_3$-TC_{NaOH} with different particle size on As(V) were investigated, and the results are shown in Fig. 4.

As shown in Fig. 4, the removal rate of As(V) increased with the decrease of the particle size of the adsorbent, from 36.2% with particle size of 125–150 μm to 85.3% with particle size < 61 μm, indicating that the particle size of the adsorbent has a great influence on the adsorption of $Fe(OH)_3$-TC_{NaOH} to As(V). $Fe(OH)_3$-TC_{NaOH} with a particle size < 61 μm has the best ability to remove As(V) because the smaller the particle size of the adsorbent, the larger the specific surface area, and $Fe(OH)_3$-TC_{NaOH} with a particle size < 61 μm can be dispersed in solution for a longer time (as shown in Fig. 3), allowing the adsorbent to fully contact the active site of the adsorbent. But on the other hand, precisely because it is dispersed in solution for a long time, it has the worst precipitation effect, resulting in difficult to separate from water at the end of adsorption. $Fe(OH)_3$-TC_{NaOH} with particle sizes of 61–67 μm and 67–75 μm not only have higher As(V) removal rates (76.3 and 69.8%, respectively), but also have better sedimentation performance.

In order to meet the needs of mass production and facilitate comparison, 61–75 μm (combining 61–67 μm and 67–75 μm) and < 61 μm were selected for subsequent experiments.

Effect of reaction time on adsorption of As(V) by $Fe(OH)_3$-TCNaOH

The effect of reaction time on the adsorption of As(V) by $Fe(OH)_3$-TC_{NaOH} with particle sizes of 61–75 μm and < 61 μm were studied, the results are shown in Fig. 5.

It can be seen from Fig. 5 that for $Fe(OH)_3$-TC_{NaOH} adsorbent with particle sizes of 61–75 μm and < 61 μm, the removal rate of As(V) increased rapidly in the first 20 min of the reaction. That is because at the beginning of the reaction, there is a large concentration difference between As(V) in solution and the surface of the adsorbent, and As(V) rapidly diffuses to the surface of adsorbent and binds to the adsorption site. With the process of adsorption, the removal rate of As(V) gradually increased until the adsorption equilibrium was reached. The As(V) removal rate of adsorbents with particle size < 61 μm reached 90% at 15 min, that is, the effluent As(V) content was 0.5 mg/L, which met the requirements of Integrated Wastewater Discharge Standard of the People's Republic of China (GB 8978 − 1996). The As(V) removal rate of adsorbents with particle size of 61–75 μm reached 90% at 30 min. Considering the time cost, the adsorption time was selected as 30 min in subsequent experiments.

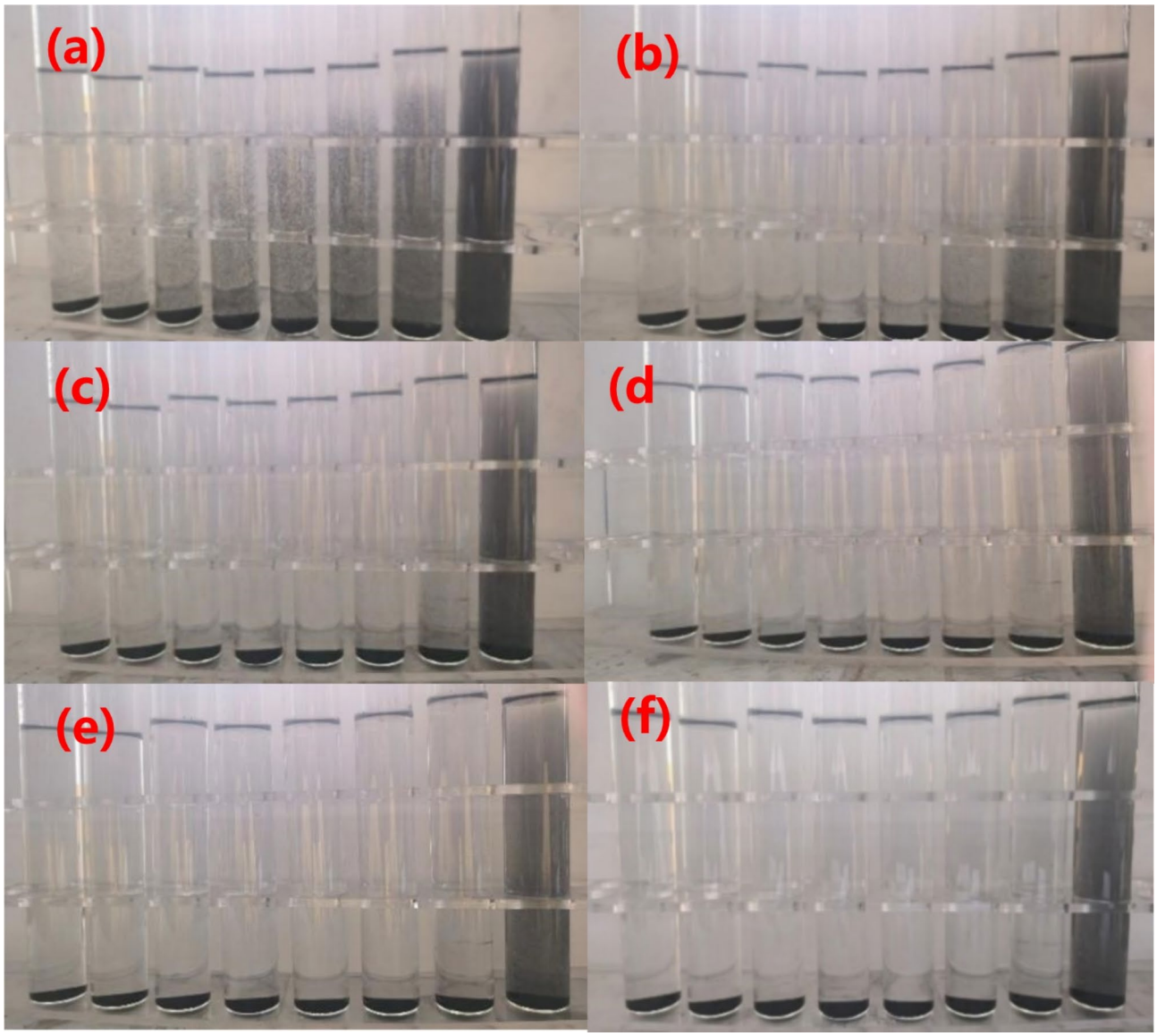

Fig. 3. Settleability of $Fe(OH)_3$-TC_{NaOH} with different particle sizes in DI water (the size of $Fe(OH)_3$-TC_{NaOH} from left to right in each figure ranges from 125 to 150 μm to < 61 μm. Figure (**a**) was left standing for 0 min. Figure (**a-f**) show the results of a 1 min standing interval).

Effect of pH in solution on adsorption of As(V) by $Fe(OH)_3$-TCNaOH

The effect of solution pH on the adsorption of As(V) by $Fe(OH)_3$-TC_{NaOH} with particle sizes of 61–75 μm and < 61 μm is shown in Fig. 6.

As can be seen from Fig. 6, solution pH is an important factor affecting the adsorption of As(V). In the range of pH 3–9, the removal rate of As(V) for $Fe(OH)_3$-TC_{NaOH} with a particle size of 61–75 μm was always about 90%, while for $Fe(OH)_3$-TC_{NaOH} with a particle size of < 61 μm, the removal rate of As(V) remained above 96%. The results showed that $Fe(OH)_3$-TC_{NaOH} with two particle sizes had higher As(V) removal rates in a wide pH range (3–9). However, the adsorption effect of the two particle sizes of $Fe(OH)_3$-TC_{NaOH} on As(V) decreased sharply when the pH value of the solution was increased (10–11). When the pH value was 9–11, the removal efficiency of As(V) by $Fe(OH)_3$-TC_{NaOH} with two particle sizes was reduced by more than 70%.

The above phenomenon can be explained by the presence of As(V) and Fe(III) in the solution. When the solution pH is 3–7, the surface functional groups of $Fe(OH)_3$-TC_{NaOH} are protonated, the loaded Fe(III) mainly exists in the form of positively charged $Fe(OH)^{2+}$, while As(V) exists mainly in the form of negatively charged $AsO_2(OH)_2^-$. At this time, the adsorbate is combined with the adsorbent under electrostatic attraction, and As(V) is protonated or complexed on the surface of $Fe(OH)_3$-TC_{NaOH}, and acts as a H bond donor to form a double-toothed binuclear surface complex (as shown in Eq. (1)). The formation of H bond is beneficial to the adsorption of $Fe(OH)_3$-TC_{NaOH} to As(V) and increases the stability of Fe-As complex[31].

$$2Fe(OH)^{2+} + AsO_2(OH)_2^- + H^+ \rightarrow (FeO)_2AsO(OH) + 2H_2O \quad (1)$$

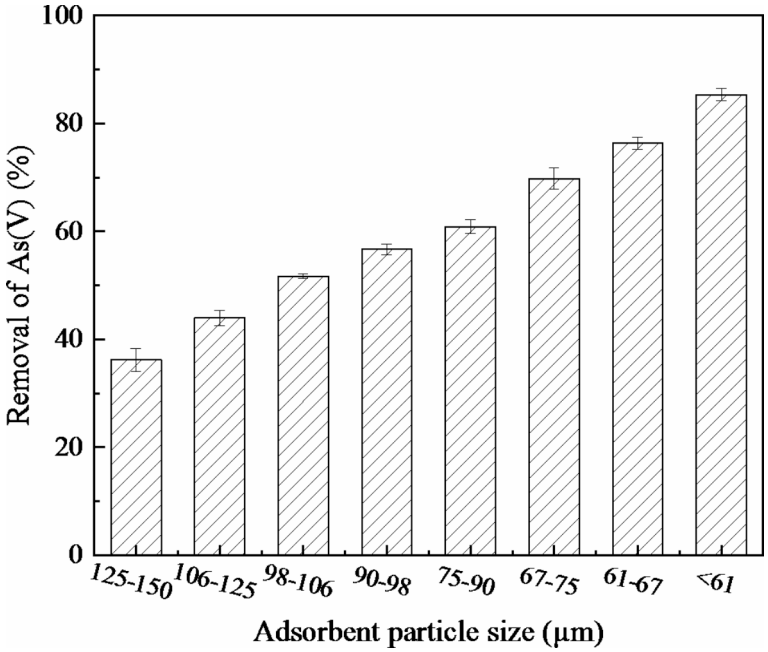

Fig. 4. Effect of adsorbent particle size on adsorption of As(V) by $Fe(OH)_3$-TC_{NaOH} (initial concentration of As(V) was 5 mg/L, pH in solution 9, dosage of adsorbent 0.8 g/L, reaction temperature 25 °C, reaction time 10 min).

In the range of pH 7–9, the surface functional groups of $Fe(OH)_3$-TC_{NaOH} are deprotonated, and the loaded Fe(III) is gradually transformed into $Fe(OH)_4^-$, while As(V) is into $AsO_3(OH)^{2-}$, which is more electronegative. At this moment, the electrostatic attraction between the adsorbate and the adsorbent gradually weakens, and As(V) is deprotonated on the surface of $Fe(OH)_3$-TC_{NaOH} and becomes an H bond receptor, forming a small number of single-tooth bond[32–34], as shown in Eq. (2).

$$Fe(OH)_4^- + AsO_3(OH)^{2-} + OH^- \rightarrow FeOAsO_4(OH)_2 + 2H_2O \quad (2)$$

At pH 9–11, Fe(III) mainly exists in the form of $Fe(OH)_4^-$, and As(V) is further transformed into AsO_4^{3-}. At this time, the electrostatic repulsion between the adsorbate and the adsorbent gradually increases, and AsO_4^{3-} cannot contact the Fe-O group on the surface of $Fe(OH)_3$-TC_{NaOH}, making it difficult to carry out chemisorption behavior, resulting in a precipitous decline in the adsorption effect of $Fe(OH)_3$-TC_{NaOH} on As(V).

Effect of initial concentration and reaction temperature on the adsorption of As(V) by $Fe(OH)_3$-TCNaOH

The effect of initial concentration and reaction temperature on the adsorption of As(V) by $Fe(OH)_3$-TC_{NaOH} with particle size 61–75 μm and < 61 μm are shown in Fig. 7.

As can be seen from Fig. 7, the adsorption capacity of $Fe(OH)_3$-TC_{NaOH} to As(V) increased with the increase of reaction temperature, indicating that the adsorption process of $Fe(OH)_3$-TC_{NaOH} to As(V) may be endothermic. In particular, when the initial concentration of As(V) was 4 mg/L and the reaction temperature increased from 25 °C to 45 °C, the adsorption capacity of $Fe(OH)_3$-TC_{NaOH} with particle sizes of 61–75 μm and < 61 μm increased from 2.78 to 3.58 mg/g to 4.47 and 5.52 mg/g, respectively. However, when the reaction temperature was increased from 45 °C to 55 °C, adsorption capacity of the two particle sizes of $Fe(OH)_3$-TC_{NaOH} was basically not different from that at 45 °C.

In addition, it can also be seen from Fig. 7 that the adsorption capacity of $Fe(OH)_3$-TC_{NaOH} with a particle size < 61 μm was always higher than that of $Fe(OH)_3$-TC_{NaOH} with particle size of 61–75 μm at the studied reaction temperature (25–55 °C).

Table 1 summarizes the arsenic adsorption capacity by different adsorbents. As can be seen from Table 1, $Fe(OH)_3$-TC_{NaOH} can achieve a high removal rate in a shorter time. The relatively low adsorption capacity of $Fe(OH)_3$-TC_{NaOH} for As(V) is due to the low initial As(V) concentration. Therefore, in the removal of low concentration As(V), $Fe(OH)_3$-TC_{NaOH} is a very good option.

Effect of co-existing ions on adsorption of As(V) by $Fe(OH)_3$-TCNaOH

Based on the coexistence of multiple cations and anions in actual wastewater, these co-existing ions may interfere with the adsorption of $Fe(OH)_3$-TC_{NaOH} to As(V). Since the pH of the solution was controlled at 9 in this study, most metal cations exist in the form of precipitate at this pH condition. Five ions (NH_4^+, Ca^{2+}, Cl^-, CO_3^{2-} and PO_4^{3-}) with an ion concentration of 5 mg/L were added to As(V)-containing solution, respectively, to study the effect of coexisting ion on adsorption of As(V) by $Fe(OH)_3$-TC_{NaOH}, as shown in Fig. 8.

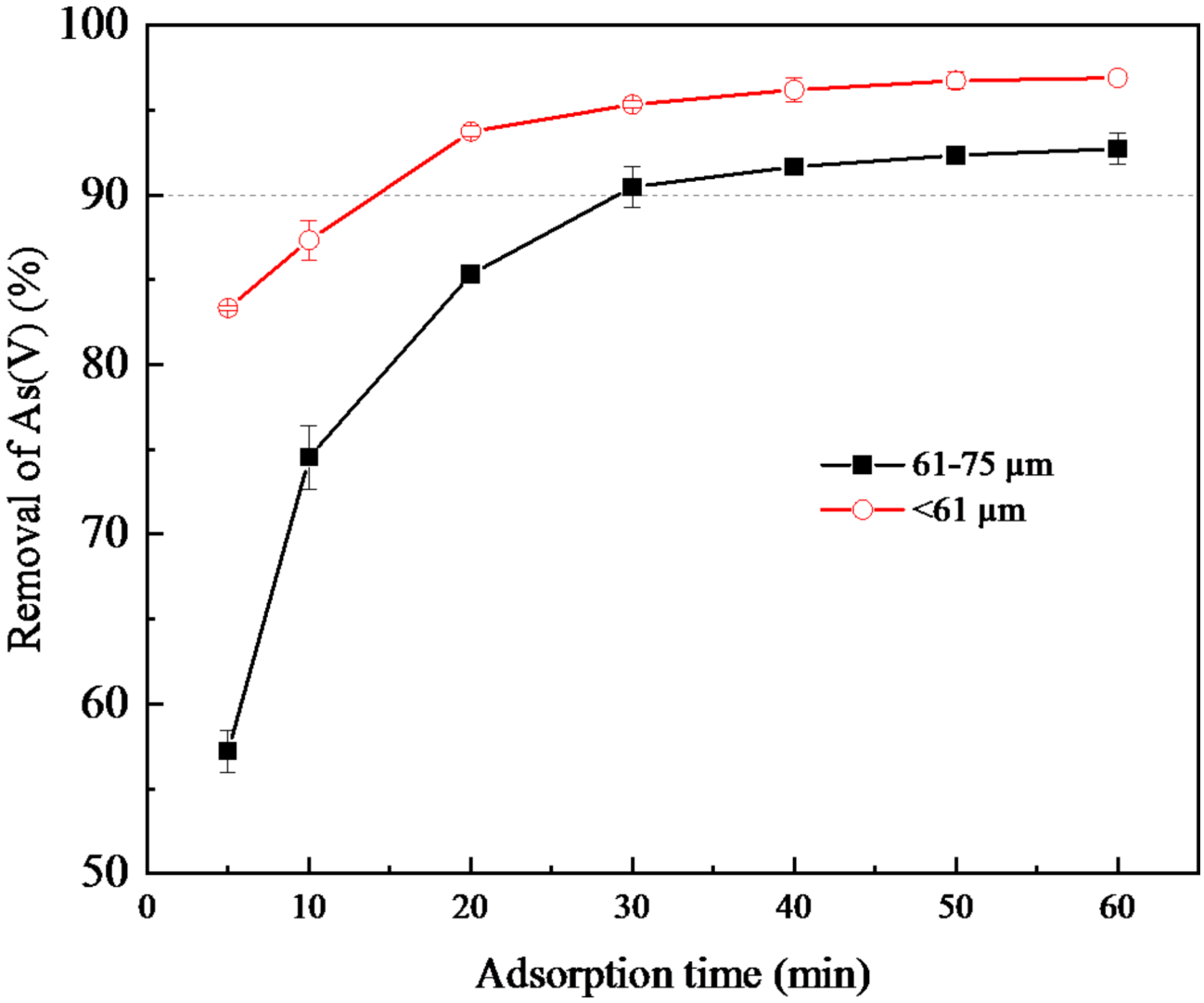

Fig. 5. Effect of reaction time on adsorption of As(V) by $Fe(OH)_3$-TC_{NaOH} (initial concentration of As(V) was 5 mg/L, pH in solution 9, dosage of adsorbent 0.8 g/L, reaction temperature 25 °C).

From Fig. 8 can be seen that when NH_4^+, Ca^{2+}, Cl^- and CO_3^{2-} of 5 mg/L coexist, the removal rate of As(V) by $Fe(OH)_3$-TC_{NaOH} of the two particle sizes (61–75 μm and < 61 μm) was almost unchanged, indicating that the adsorption capacity of $Fe(OH)_3$-TC_{NaOH} to As(V) was almost unaffected by these ions. In contrast, the effect of PO_4^{3-} on the adsorption of As(V) by $Fe(OH)_3$-TC_{NaOH} was very significant, that is, the removal rates of $Fe(OH)_3$-TC_{NaOH} with particle sizes of 61–75 μm and < 61 μm decreased from 90.1 to 96.2% to 62.3 and 74.4%, respectively. This is because the spatial structure of PO_4^{3-} is similar to that of AsO_4^{3-}, resulting in PO_4^{3-} competing with AsO_4^{3-} for the active site on the surface of $Fe(OH)_3$-TC_{NaOH} and possibly reacting with Fe^{3+} to form the precipitate of $FePO_4$. On the other hand, even if the concentration of coexisting PO_4^{3-} and As(V) was the same, the removal efficiency of $Fe(OH)_3$-TC_{NaOH} with two particle sizes for As(V) was greater than 60%, which further indicates that $Fe(OH)_3$-TC_{NaOH} has a strong adsorption effect on As(V).

Characterization of adsorbent

Pore size and specific surface area of the adsorbent

The pore sizes and specific surface area of TC, TC_{NaOH} and $Fe(OH)_3$-TC_{NaOH} with two particle sizes (61–75 μm and < 61 μm) were compared, as shown in Table 2.

It can be seen from Table 2 that the pore volume of the four materials is similar, about 0.11 cm^3/g. Among the three materials, the largest average pore size (6.91 nm) and the smallest specific surface area (68.6 m^2/g) of TC explain the reason why the removal rate of TC for As(V) was the lowest in Fig. 2. The pore size of TC_{NaOH} (6.46 nm) is smaller than that of TC (6.91 nm), which means that the modification of NaOH increased the specific surface area of TC (from 68.6 to 74.8 m^2/g). The specific surface areas of $Fe(OH)_3$-TC_{NaOH} with 61–75 μm and < 61 μm are 82.6 and 84.4 m^2/g, respectively, which were much higher than the 6.46 nm of TC_{NaOH}, indicating that the specific surface area of TC was further improved by iron modification. The smallest pore

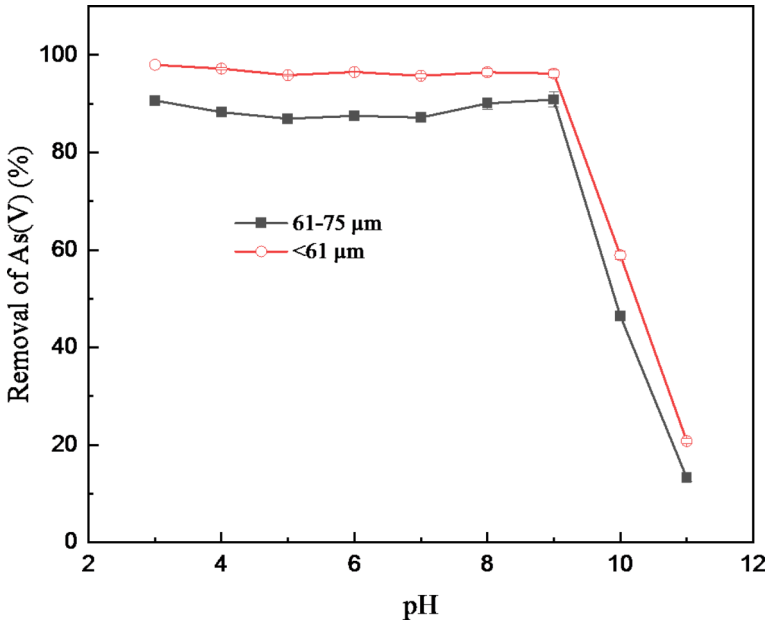

Fig. 6. Effect of pH in solution on adsorption of As(V) by $Fe(OH)_3$-TC_{NaOH} (initial concentration of As(V) was 5 mg/L, dosage of adsorbent 0.8 g/L, reaction time 30 min, reaction temperature 25 °C).

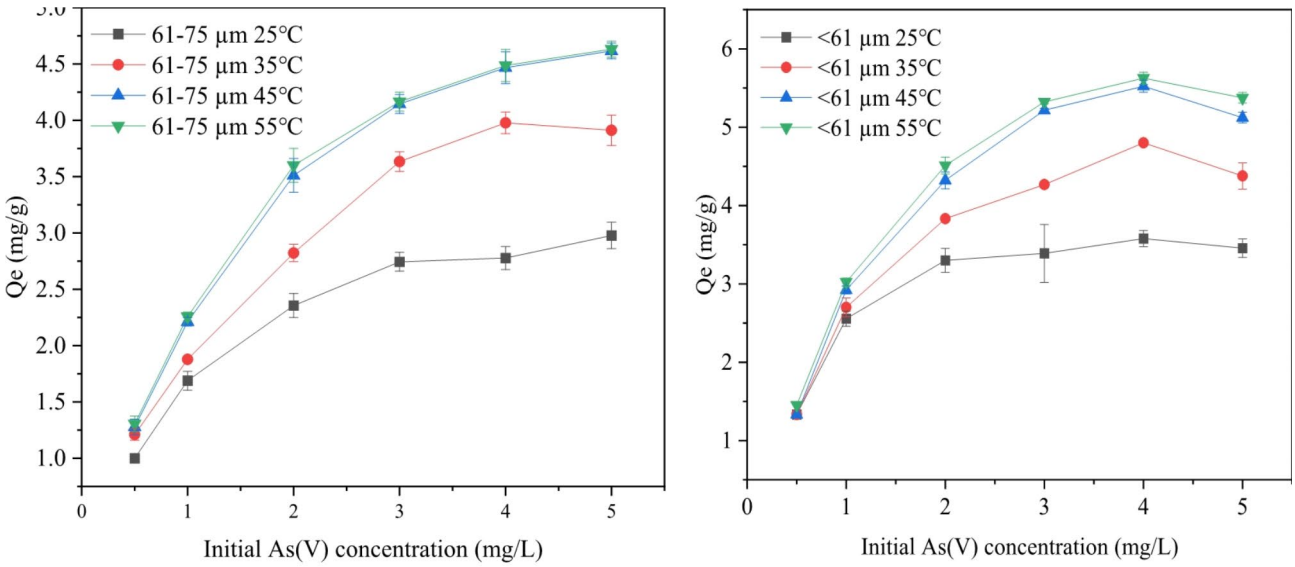

Fig. 7. Effect of initial concentration and reaction temperature on the adsorption of As(V) by $Fe(OH)_3$-TC_{NaOH} (initial concentration of As(V) was 0.5-5 mg/L, pH in solution 9, dosage of adsorbent 0.8 g/L, reaction time 30 min, reaction temperature 25–45 °C).

size and the largest specific surface area make $Fe(OH)_3$-TC_{NaOH} with particle size < 61 μm the best removal performance of As(V).

Figure 9 shows the N_2 adsorption/desorption curves and pore size distribution of the three adsorbents. It can be seen that the type of N_2 adsorption/desorption isotherms of the three materials are the same, similar to type IV isotherms with H3 hysteresis loops, showing the characteristics of mesoporous materials. The adsorption process begins with the formation of single or multiple layers on the surface of the material, followed by pore

Adsorbent	Initial pH	Adsorption capacity	Equilibrium time	Valence state of arsenic
Amine-doped acrylic ion exchange fiber [35]	3.04	100.35 mg/g	60 min	As(V)
Modacrylic anion exchange fiber [36]	7.5–8.6	0.346 mmol/g	180 min	As(V)
This study	9	5.52 mg/g	30 min	As(V)
Fe-impregnated food waste biochar [37]	7.0	119.5 mg/g	60 min	As(III)
Aluminum-Modified Food Waste Biochar [38]	11	52.2 mg/g	24 h	As(III)

Table 1. Arsenic adsorption capacities of different adsorbents.

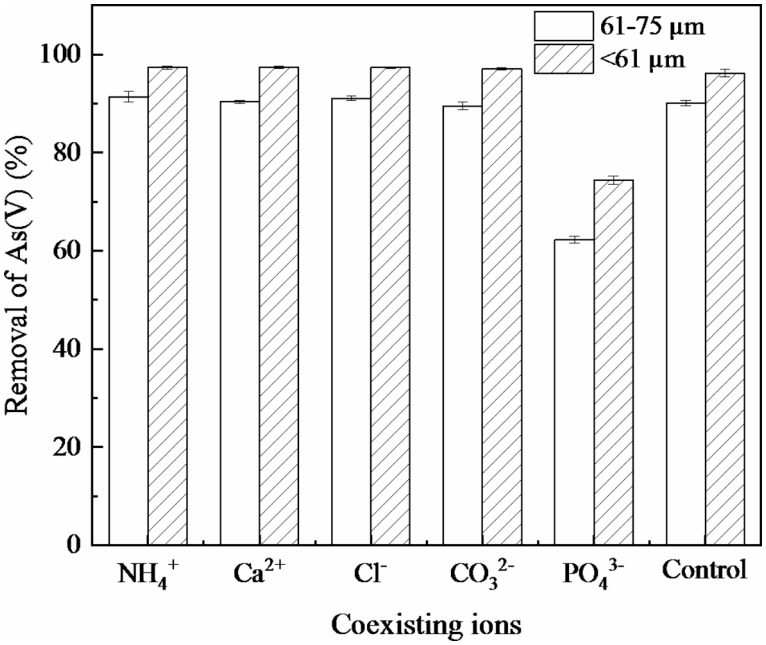

Fig. 8. Effect of coexisting ions on adsorption of As(V) by $Fe(OH)_3$-TC_{NaOH} (initial concentration of As(V) was 5 mg/L, coexisting ion concentration 5 mg/L, pH in solution 9, dosage of adsorbent 0.8 g/L, reaction time 30 min, reaction temperature 25 °C).

Sample	Pore volume (cm^3/g)	Aperture (nm)	Specific surface area (m^2/g)
TC	0.11	6.91	68.6
TC_{NaOH}	0.11	6.46	74.8
$Fe(OH)_3$-TC_{NaOH} with 61–75 μm	0.10	5.32	82.6
$Fe(OH)_3$-TC_{NaOH} with < 61 μm	0.11	4.93	84.4

Table 2. The pores size and specific surface area for three adsorbents.

condensation. There is no obvious saturated adsorption platform in the hysteresis loop, indicating that the pore structure is very irregular.

It can be seen from the pore size distribution in Fig. 9 that the main peak positions of the three materials are similar. In the range of 10–70 nm, the overall peak shape is wide, indicating that the pore size distribution of the material is not uniform, which is consistent with the hysteresis loop of N_2 adsorption/desorption curve. The pore size of TC is mainly distributed in the range of 9–70 nm, among which the pore size of 35 nm is the most abundant, and a small number of micropores (< 2 nm) are also contained. Compared with TC, the number of 3–5 nm mesoporous pores of $Fe(OH)_3$-TC_{NaOH} of the two particle sizes increased significantly, while the number of pores above 20 nm decreased significantly, indicating that the modification process changed the pore structure of TC. This is consistent with the results in Table 1.

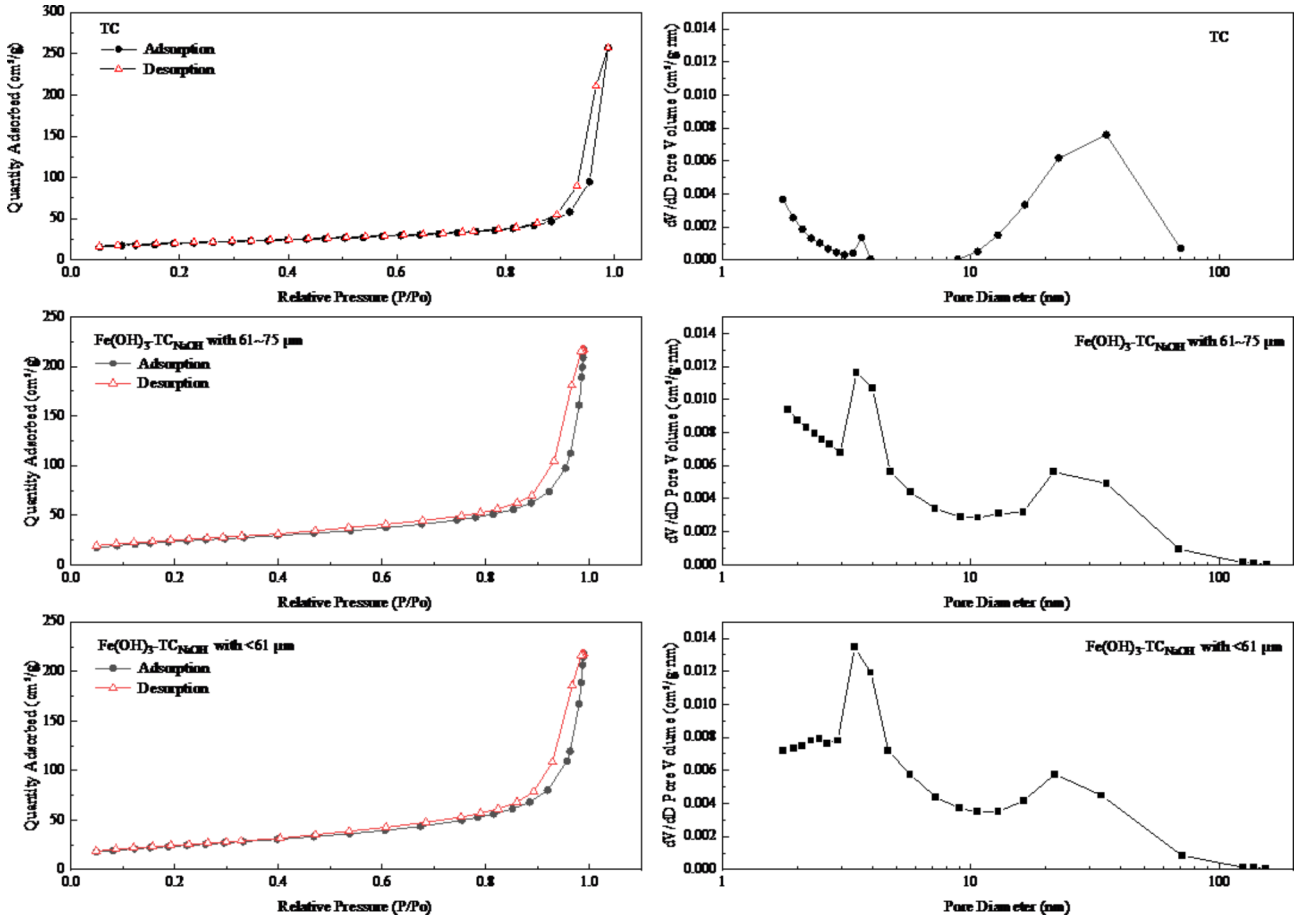

Fig. 9. N_2 sorption/desorption curves (left) and pore size distributions (right) for TC and $Fe(OH)_3$-TC_{NaOH}.

Phase analysis

The phase analysis of TC, $Fe(OH)_3$-TC_{NaOH} (particle size 61–75 μm) and $Fe(OH)_3$-TC_{NaOH}-As(V) was carried out to determine the surface structure changes before and after TC modification and after adsorption of As(V). The results are shown in Fig. 10.

All three materials in Fig. 10 have a distinct hump at 25°, which is a typical of a wide graphitic carbon peak. The peak intensity indicates that the crystallinity of carbon in the three materials is poor, indicating that the main component is amorphous carbon[29]. The characteristic peaks of ZnS crystals are at 27°, 28°, 30°, 39°, 47° and 57° on TC, respectively. The ZnS phase is formed by the reaction between S in the vulcanization process[29] of tire production and ZnO added in tire production during the pyrolysis of waste tires[39,40]. The characteristic peaks of SiO_2 crystals are at 21°, 27°, 36° and 42° on TC, respectively. SiO_2, which has a decomposition temperature of 1713 °C, is a commonly used additive in tire production, and it is difficult to decompose SiO_2 during the pyrolysis process of waste tire, so it is converted into pyrolysis char[40]. It can also be noted that in Fig. 10, $Fe(OH)_3$-TC_{NaOH} has no obvious diffraction peaks of iron-containing compounds, indicating that $Fe(OH)_3$-TC_{NaOH} has poor crystallinity. After $Fe(OH)_3$-TC_{NaOH} adsorbed As(V), the crystallinity is not good even if a new substance is formed[41].

Compared with TC, the graphite peak intensity of $Fe(OH)_3$-TC_{NaOH} and $Fe(OH)_3$-TC_{NaOH}-As(V) decreased significantly at 25°, and the characteristic peak intensity of ZnS also decreased significantly. This may be because the loaded iron forms a layer of iron-containing compounds with low crystallinity on the surface of the char. Similarly, SiO_2 peaks in $Fe(OH)_3$-TC_{NaOH} and $Fe(OH)_3$-TC_{NaOH}-As(V) are significantly reduced compared to TC because the NaOH modification process removes most of the SiO_2.

Energy spectrum analysis

The energy spectrum analysis of TC, $Fe(OH)_3$-TC_{NaOH} (particle size 61–75 μm) and their adsorption of As(V) is shown in Fig. 11.

Figure 11(a) shows the atomic ratios of C, O, Al, Si, S, Ca, Fe, Zn, and As in TC. Compared with Fig. 11(a), the ratio of Fe and O atoms in $Fe(OH)_3$-TC_{NaOH} in Fig. 11(b) increased from 0.10 to 10.25% to 4.55 and 37.40%, respectively, indicating that Fe elements were successfully loaded on the surface of char in the form of iron oxide. Compared with Fig. 11(a), the As atom ratio in TC-As(V) (Fig. 11(c)) increased from 0 to 0.16%, indicating that a small amount of As was adsorbed on the TC surface. Similarly, compared with Fig. 11(b), the As atom ratio

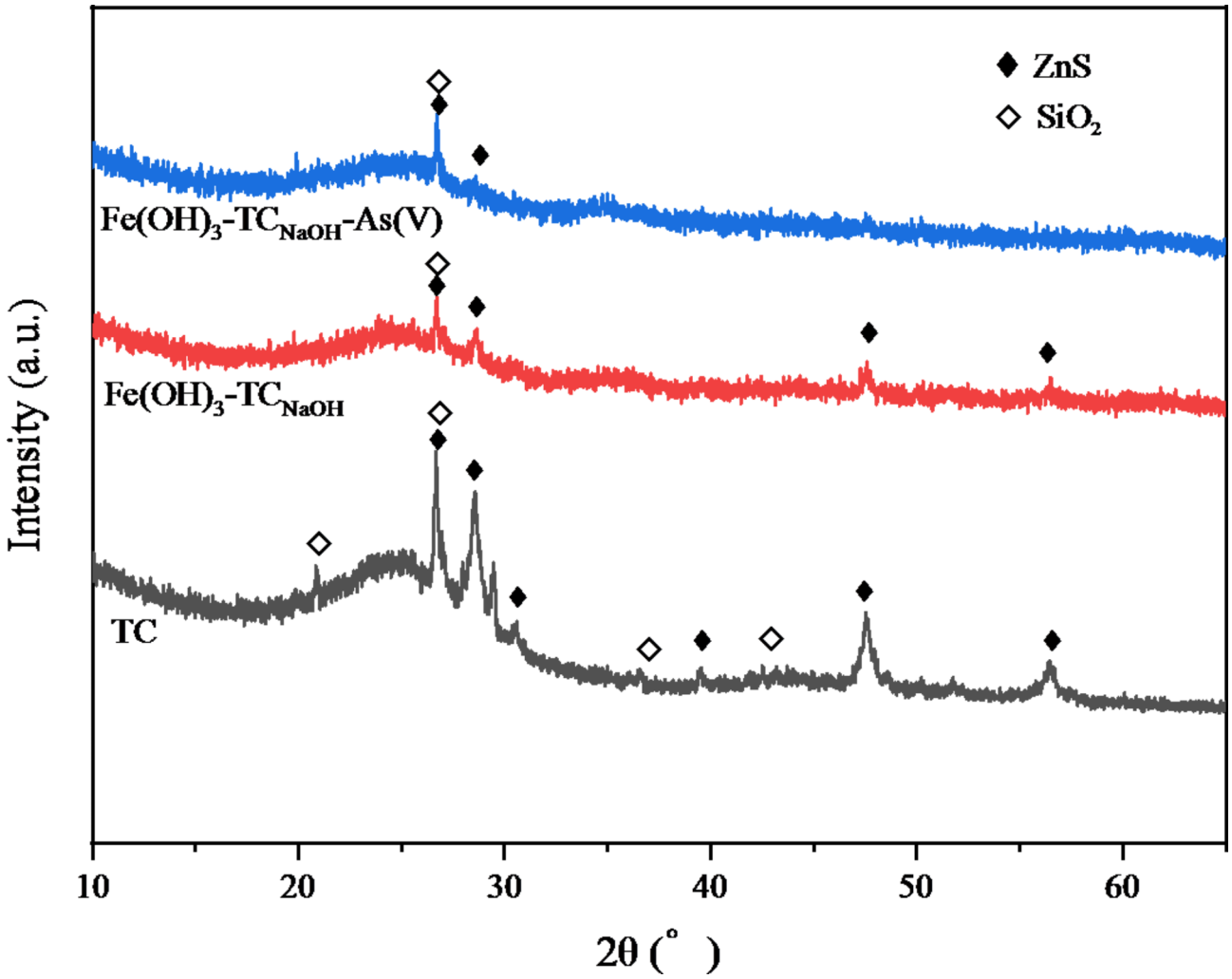

Fig. 10. Phase analysis of TC, $Fe(OH)_3$-TC_{NaOH} and $Fe(OH)_3$-TC_{NaOH}-As(V).

in $Fe(OH)_3$- TC_{NaOH}-As(V) (Fig. 11(d)) increased from 0 to 0.85%, indicating that As(V) was adsorbed on the surface of $Fe(OH)_3$-TC_{NaOH}.

X-ray photoelectron spectroscopy (XPS) analysis

In order to further clarify the adsorption mechanism of As(V), the surface elemental states of TC and $Fe(OH)_3$-TC_{NaOH} (particle size 61–75 μm) before and after adsorption were analyzed by XPS), as shown in Fig. 12.

As shown in Fig. 12, the four samples exhibit the same peaks around 92.7, 142.2, 283.2, 531.5 and 1020.7 eV, corresponding to Si 2p, S 2p, C 1s, O 1s and Zn 2p respectively. It means that there are Si, S, C, O and Zn elements in TC and $Fe(OH)_3$-TC_{NaOH}, and there is basically no change after adsorption of As(V), which is consistent with Xu[41]. In the spectra of $Fe(OH)_3$-TC_{NaOH} and $Fe(OH)_3$-TC_{NaOH}-As(V), the characteristic peak of Fe 2p can be clearly seen at about 710 eV. In addition, $Fe(OH)_3$-TC_{NaOH}-As(V) showed a new peak around 45.1 eV in As 3d, which confirmed the transfer of As(V) from the liquid phase to the surface of $Fe(OH)_3$-TC_{NaOH}. However, As 3d in TC-As(V) is very weak near 45 eV, which is consistent with the results in Fig. 2, that is, $Fe(OH)_3$-TC_{NaOH} has a much better adsorption effect on As(V) than TC.

XPS spectra changes of C, O, Fe and As were further studied, and the results were shown in Figs. 13 and 14.

Figure 13 shows that the C1s spectra of TC and TC-As(V) include two peaks corresponding to sp2 hybrid carbon (C=C) at 284.0 eV and C-O at 285.8 eV. C=C dominated in TC and TC-As(V), with 89.1% and 92.9%, respectively. The C1s spectra of $Fe(OH)_3$-TC_{NaOH} and $Fe(OH)_3$-TC_{NaOH}-As(V) consist of three peaks, corresponding to C=C, C-O, C=O at 284.0, 285.9, 288.9 eV, respectively. The contents of these three kinds of carbon in $Fe(OH)_3$-TC_{NaOH} and $Fe(OH)_3$-TC_{NaOH}-As(V) are 74, 18.8, 7.2% and 80.4, 15.8, 3.8%, respectively. Both TC and $Fe(OH)_3$-TC_{NaOH} contain more sp2 carbon (89.1 and 74% respectively), indicating that the degree of graphitization is higher, and the surface of $Fe(OH)_3$-TC_{NaOH} contains more oxygen functional groups than that of TC.

As can be seen from Fig. 14(a), the O 1s spectrum of $Fe(OH)_3$-TC_{NaOH} can be divided into three peaks of 529.5, 531.2 and 532.6 eV, belonging to Fe-O, Fe-OH and H-O-H, with intensities of 31.8, 48.9 and 19.3%, respectively[42,43]. The strength of Fe-OH peaks is greater than that of the other two oxygen-containing structures,

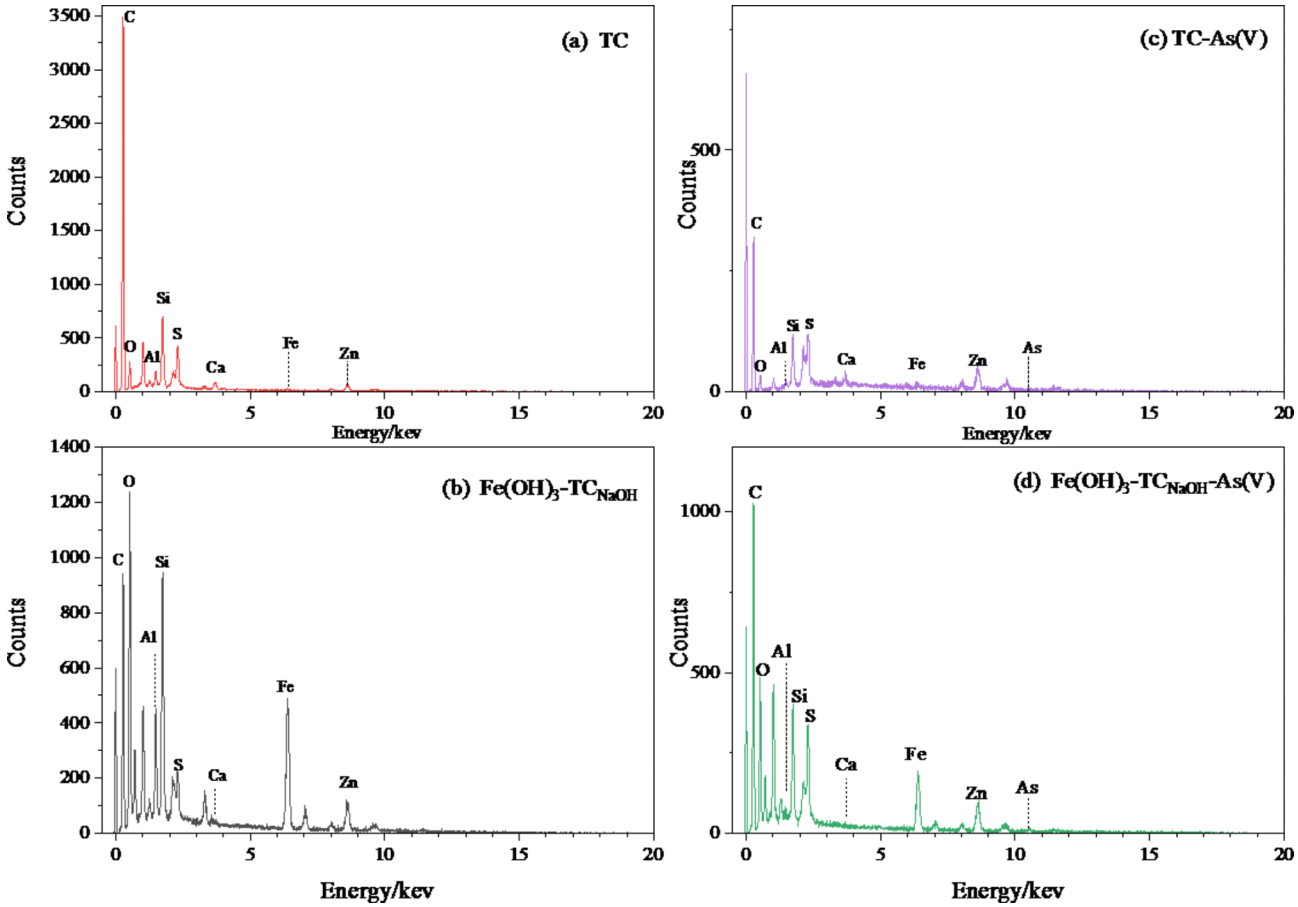

Fig. 11. Energy spectrum analysis.

indicating that $Fe(OH)_3$-TC_{NaOH} surface is dominated by Fe-OH. In the O 1s spectrum after adsorption of As(V), the peak strength of Fe-OH decreased from 48.9 to 44.3%, while the peak strength of Fe-O increased from 31.8 to 36.4%, indicating that hydroxyl group participated in the surface chemisorbed process and formed a new complex Fe-O-As through exchange with Fe-OH ligand[44,45].

As shown in Fig. 14(b), the Fe 2p spectrum of $Fe(OH)_3$-TC_{NaOH} has two prominent peaks at 710.7 and 724.4 eV, corresponding to Fe $2p_{3/2}$ and Fe $2p_{1/2}$, respectively. Since the satellite peak of the binding energy of 720 eV corresponds to Fe(III), it means that Fe exists as Fe(III) in $Fe(OH)_3$-TC_{NaOH}. The Fe $2p_{3/2}$ and Fe $2p_{1/2}$ spectra of $Fe(OH)_3$-TC_{NaOH}-As(V) are located at 709.8 and 723.2 eV, respectively, that is, the binding energy of Fe 2p is slightly lower than that of $Fe(OH)_3$-TC_{NaOH}, indicating that Fe participates in the adsorption reaction[46].

From Fig. 14(c) can be seen that As 3d can decompose two peaks at 43.1 and 45.0 eV, corresponding to As(III) and As(V), respectively, with intensities of 11 and 89%, indicating that it is mainly adsorbed on the surface of $Fe(OH)_3$-TC_{NaOH} in the form of As(V). During XPS detection, a small amount of As(III) may be partially reduced to As(III) by ZnS on the surface $Fe(OH)_3$-TC_{NaOH} and X-ray[47]. When pH is 9, the loaded Fe(III) on the surface of $Fe(OH)_3$-TC_{NaOH} and adsorbed As(V) may undergo a single-tooth complex reaction, as shown in the following Eq. (2).

Conclusions

In line with the idea of "treating waste with waste", TC was modified at room temperature and air atmosphere to obtain $Fe(OH)_3$-TC_{NaOH} adsorbent. The influencing factors and mechanism of removal of As(V) by adsorbent were studied systematically. The removal rate of As(V) by $Fe(OH)_3$-TC_{NaOH} modified with iron salt after alkali modified TC is higher than other modification methods. The particle size of $Fe(OH)_3$-TC_{NaOH} is inversely proportional to the sedimentation performance and proportional to the removal performance of As(V). The As(V) removal rate of $Fe(OH)_3$-TC_{NaOH} with particle size of 61–75 μm can reach 90% in 30 min at a wide pH range (3–9). In the experiment of coexistence ion effect, PO_4^{3-} has the greatest interference on $Fe(OH)_3$-TC_{NaOH} adsorption of As(V), resulting in a decrease in the removal rate of As(V). The adsorption mechanism shows that the significant increase in the number of 3–5 nm mesoporous pores of $Fe(OH)_3$-TC_{NaOH} and the formation of H bonds are beneficial to the adsorption of $Fe(OH)_3$-TC_{NaOH} to As(V), and improve the stability of Fe-As complex.

Future research will focus on the desorption, regeneration and recycling of $Fe(OH)_3$-TC_{NaOH} adsorbents.

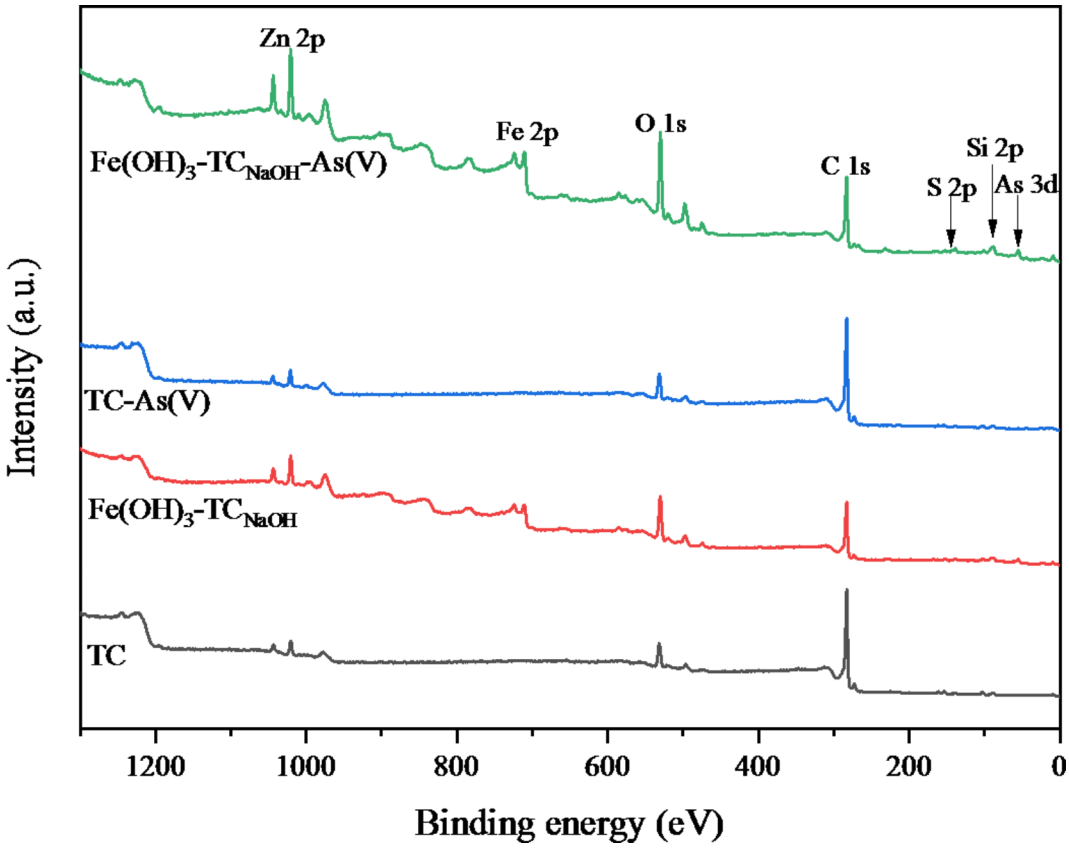

Fig. 12. XPS total spectra of TC and $Fe(OH)_3$-TC_{NaOH} before and after As(V) adsorption.

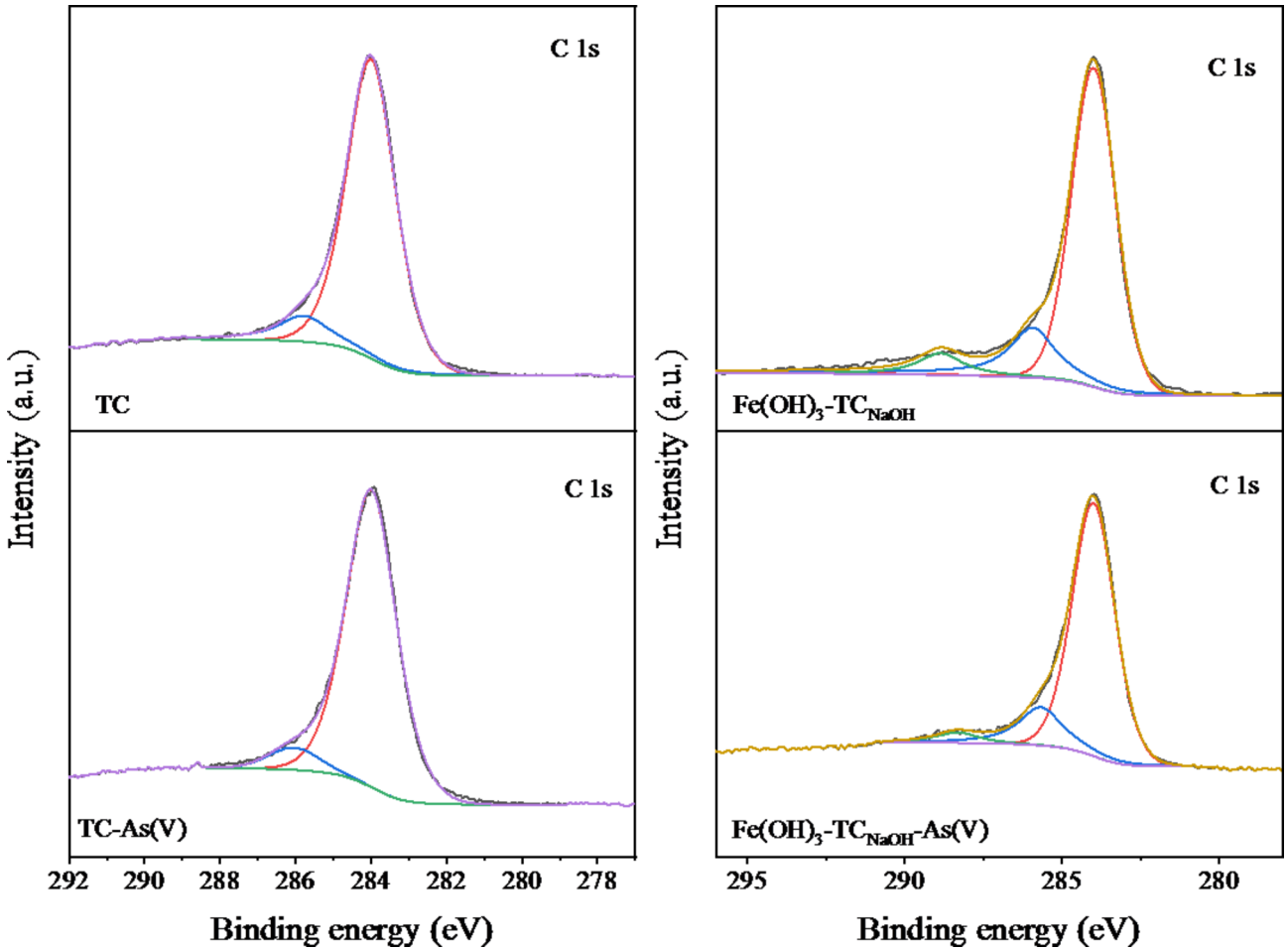

Fig. 13. Spectrum changes of XPS C1s before and after adsorption of As(V) by TC and $Fe(OH)_3$-TC_{NaOH}.

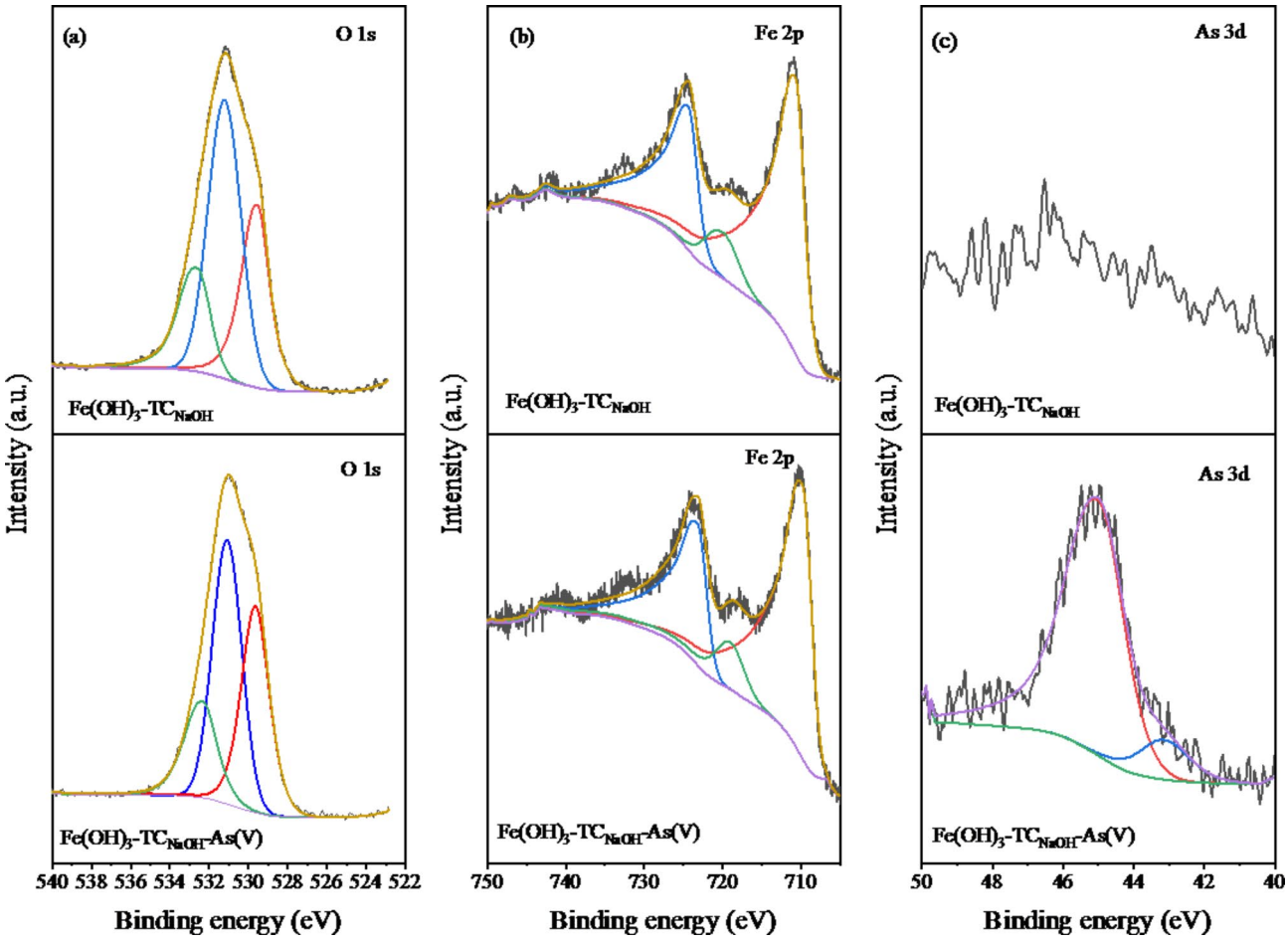

Fig. 14. Spectra changes of XPS (**a**) O 1s, (**b**) Fe 2p and (**c**) As 3d before and after $Fe(OH)_3$-TC_{NaOH} adsorption of As(V).

Data availability

Data is provided within the supplementary information files.

Received: 8 August 2024; Accepted: 24 September 2024
Published online: 04 October 2024

References

1. Weibo Consulting. *China Waste Tire Recycling Industry Research and In-depth Analysis Report. 2023*. (2023).
2. Brandsma, S. H. et al. Chlorinated paraffins in car tires recycled to rubber granulates and playground tiles. *Environ. Sci. Technol.* **53**, 7595. https://doi.org/10.1021/acs.est.9b01835 (2019).
3. Jaysoon, D. et al. Tire waste steel fiber in reinforced self-compacting concrete. *Chem. Eng. Trans.* **94**, 1327 (2022).
4. Li, J. *Study on Zinc Removal from Waste Tire Rubber Powder* (China University of Mining and Technology, 2019).
5. Mohan, A., Dutta, S., Balusamy, V. & Madav Liquid fuel from waste tires: Novel reffning, advanced characterization and utilization in engines with ethyl levulinate as an additive [J]. *RSC Adv.* **11**, 9807. https://doi.org/10.1039/d0ra08803j (2021).
6. Anmol, S., Chandresh, D. & Sampatrao, M. Experimental and theoretical investigation on pyrolysis of various sections of the waste tire and its components. *Chem. Eng. Res. Des.* **179**, 66–76. https://doi.org/10.1016/j.cherd.2021.12.022 (2022).
7. Watterson, A. Artificial turf: Contested terrains for precautionary public health with particular reference to Europe? *Int. J. Environ. Res. Public Health.* **14** (9), 1050. https://doi.org/10.3390/ijerph14091050 (2017).
8. Labaki, M. & Jeguirim, M. Thermochemical conversion of waste tyres—A review. *Environ. Sci. Pollut. R.* **24** (11), 9962. https://doi.org/10.1007/s11356-016-7780-0 (2017).
9. Saleh, T. & Danmaliki, G. Adsorptive desulfurization of dibenzothiophene from fuels by rubber tires-derived carbons: Kinetics and isotherms evaluation. *Process. Saf. Environ.* **102**, 9. https://doi.org/10.1016/j.psep.2016.02.005 (2016).
10. Qiao, Y. et al. Effect of demineralization on waste tire pyrolysis char physical, chemical characteristics and combustion characteristics. *Energy.* **284**, 129219. https://doi.org/10.1016/j.energy.2023.129219 (2023).
11. López, F. et al. Distillation of granulated scrap tires in a pilot plant. *J. Hazard. Mater.* **190** (1–3), 285. https://doi.org/10.1016/j.jhazmat.2011.03.039 (2011).
12. Fu, J. et al. Characteristics of the pyrolytic products and the pollutant emissions at different operating stages from a pilot waste tire pyrolysis furnace[J]. *Waste Manag.* **174**, 585. https://doi.org/10.1016/j.wasman.2023.12.023 (2024).
13. Martínez, J. et al. Carbon black recovery from waste tire pyrolysis by demineralization: production and application in rubber compounding. *Waste Manag.* **85**, 574. https://doi.org/10.1016/j.wasman.2019.01.016 (2019).

14. Doja, S., Pillari, L. K. & Bichler, L. Processing and activation of tire-derived char: A review. *Renew. Sustain. Energy Rev.* **155**, 111860. https://doi.org/10.1016/j.rser.2021.111860 (2022).
15. Ma, Y. et al. Structure optimization of pyrolysis carbon black from waste tire and its application in natural rubber composites. *Appl. Surf. Sci.* **593**, 153389. https://doi.org/10.1016/j.apsusc.2022.153389 (2022).
16. Jones, I. et al. The application of spent tyre activated carbons as low-cost environmental pollution adsorbents: A technical review. *J. Clean. Prod.* **312**, 127566. https://doi.org/10.1016/j.jclepro.2021.127566 (2021).
17. Kuśmierek, K. et al. Adsorption on activated carbons from end-of-life tyre pyrolysis for environmental applications. Part I. preparation of adsorbent and adsorption from gas phase. *J. Anal. Appl. Pyrol.* **157**, 105205. https://doi.org/10.1016/j.jaap.2021.105205 (2021).
18. Wang, Y. et al. Genesis of geogenic contaminated groundwater: as, F and I. *Crit. Rev. Environ. Sci. Technol.* **512895**, 24. https://doi.org/10.1080/10643389.2020.1807452 (2021).
19. Zhang, Q. et al. Mechanism of removal of toxic arsenic (As) from zinc sulfate solution by ultrasonic enhanced neutralization with zinc roasting dust. *Sep. Purif. Technol.* **322**, 124258. https://doi.org/10.1016/j.seppur.2023.124258 (2023).
20. Algieri, C. et al. Arsenic removal from groundwater by membrane technology: Advantages, disadvantages, and effect on human health. *Groundw. Sustain. Dev.* **19**, 100815. https://doi.org/10.1016/j.gsd.2022.100815 (2022).
21. Srivastava, S. et al. Effect of combinations of aquatic plants (Hydrilla, Ceratophyllum, Eichhornia, Lemna and Wolffia) on arsenic removal in field conditions. *Ecol. Eng.* **73**, 297. https://doi.org/10.1016/j.ecoleng.2014.09.029 (2014).
22. Hakizimana, J. N. et al. Electrocoagulation process in water treatment: A review of electrocoagulation modeling approaches . *Desalination*. **404**, 1. https://doi.org/10.1016/j.desal.2016.10.011 (2017).
23. Weerasundara, L., Ok, Y. & Bundschuh, J. Selective removal of arsenic in water: A critical review. *Environ. Pollut.*. **268**, 115668. https://doi.org/10.1016/j.envpol.2020.115668 (2021).
24. Chen, Y. et al. The treatment of trace as (III) from water by modified spent grain. *Desalin. Water Treat.* **53**, 1371. https://doi.org/10.1016/j.jes.2015 (2015).
25. Chen, Y. & Xiong, C. Adsorptive removal of As(III) ions from water using spent grain modified by polyacrylamide. *J. Environ. Sci.-China*. **45** (7), 124. https://doi.org/10.1016/j.jes.2015.11.020 (2016).
26. Susan, S. et al. Inorganic arsenic species removal from water using bone char: a detailed study on adsorption kinetic and isotherm models using error functions analysis. *J. Hazard. Mater.* **405**, 124112.https://doi.org/10.1016/j.jhazmat.2020.124112 (2021).
27. Shahrokhi-Shahraki, R. et al. High efffciency removal of heavy metals using tire-derived activated carbon vs commercial activated carbon: Insights into the adsorption mechanisms. *Chemosphere*. **264**, 128455. https://doi.org/10.1016/j.chemosphere (2021). 2020.128455.
28. Karmacharya, M. et al. Removal of as(III) and As(V) using rubber tire derived activated carbon modified with alumina composite. *J. Mol. Liq.*. **216**, 836. https://doi.org/10.1016/j.molliq.2016.02.025 (2016).
29. Mouzourakis, E. et al. Recycled-tire pyrolytic carbon made functional: A high-arsenite [As(III)] uptake material PyrC 350 °. *J. Hazard. Mater.* **326**, 177. https://doi.org/10.1016/j.jhazmat.2016.12.027 (2017).
30. Therdkiattikul, N., Giao, N. & Ratpukdi, S. Manganese removal by biofiltration using activated carbon-barium alginate-entrapped cells: Morphology, durability, settling velocity, and treatment efficiency. *Appl. Environ. Res.* **43**, 127. https://doi.org/10.35762/AER.2021.43.1.10 (2021).
31. Villalobos, M. & Antelo, J. *A Unified Surface Structural Model for Ferrihydrite: Proton Charge, Electrolyte Binding, and Arsenate Adsorption* . Vol. 2. 27139–27151 (Revista Internacional de Contaminación Ambiental, 2011).
32. Yang, Z. et al. Research progress on the stability of ferrihydrite structure and its application in arsenic fixation. *J. Agro-Environ. Sci.* **39** (3), 445. https://doi.org/10.11654/jaes.2019-1167 (2020).
33. Bompoti, N., Chrysochoou, M. & Machesky, M. Surface structure of ferrihydrite: insights from modeling surface charge. *Chem. Geol.* **464**, 34–45 (2017).
34. Hiemstra, T. Formation, stability, and solubility of metal oxide nanoparticles: Surface entropy, enthalpy, and free energy of ferrihydrite. *Geochim. Cosmochim. Acta*. **158**, 179–198 (2015).
35. Lee, C. et al. Arsenic(V) removal using an amine-doped acrylic ion exchange fiber: kinetic, equilibrium, and regeneration studies. *J. Hazard. Mater.* **325**, 223. https://doi.org/10.1016/j.jhazmat.2016.12.003 (2017).
36. Lee, S. et al. Characterization of anion exchange fiber for simultaneous removal of Cr(VI) and As(V) in mineral processing wastewater. *Desalin. Water Treat.* **135**, 247. https://doi.org/10.5004/dwt.2018.23193 (2018).
37. Lyonga, F. et al. As(III) adsorption onto Fe-impregnated food waste biochar: Experimental investigation, modeling, and optimization using response surface methodology. *Environ. Geochem. Health*. **43**, 3303. https://doi.org/10.1007/s10653-020-00739-4 (2021).
38. Hashimi, S. et al. Adsorption of arsenic from water using aluminum-modified food waste biochar: Optimization using response surface methodology. *Water*. **14**, 2712 https://doi.org/10.3390/w14172712 (2022).
39. Chigova, J. & Mudono, S. Adsorption of chromium (VI) using nano-ZnO doped scrap tire-derived activated carbon. *J. Geosci. Environ. Prot.* **9**, 121 (2022).
40. Kong, Y. et al. Carbothermal synthesis of nano-iron-carbon composites for arsenate removal from high-arsenic acid wastewater. *J. Environ. Chem. Eng.* **10** (2), 107140. https://doi.org/10.1016/j.jece.2022.107140 (2022).
41. Bai, Z. et al. Study on high-efficiency arsenic removal performance and mechanism of carbon-supported ferrihydrite adsorbent . J. Ecol. Rural Environ. **38**(3), 358–366 https://doi.org/10.19741/j.issn.1673-4831.2021 (2022).
42. Xu, L. et al. Waste bamboo framework decorated with α-FeOOH nanoneedles for effective arsenic (V/III) removal. *Sci. Total Environ.* **863**, 160951. https://doi.org/10.1016/j.scitotenv.2022.160951 (2023).
43. Li, B. Mechanisms of arsenate and cadmium co-immobilized on ferrihydrite inferred from ternary surface configuration. *Chem. Eng. J.* **424**, 130410. https://doi.org/10.1016/j.cej.2021.130410 (2021).
44. Du, Y., Zhen, S., Wang, J. et al. FeOOH-MnO_2/sepiolite and Fe_2O_3-MnO_2/ diatomite: Highly efficient adsorbents for the removal of As(V). *Appl. Clay Sci.* **222**, 106491 (2022). https://doi.org/10.1016/j.clay.2022.106491
45. Xue, Q., Ran, Y., Tan, Y. et al. Arsenite and arsenate binding to ferrihydrite organo-mineral coprecipitate: Implications for arsenic mobility and fate in natural environments. *Chemosphere*. **224**, 103 https://doi.org/10.1016/j.chemosphere.2019.02.118 (2019).
46. Huo, J., Yu, G. & Wang, J. Magnetic zeolitic imidazolate frameworks composite as an efficient adsorbent for arsenic removal from aqueous solution. *J. Hazard. Mater.* **412**, 125298. https://doi.org/10.1016/j.jhazmat.2021.125298 (2021).
47. Kong, D. et al. Characteristics and chemical treatment of carbon black from waste tires pyrolysis. *J. Anal. Appl. Pyrol.* **178**, 106419. https://doi.org/10.1016/j.jaap.2024 (2024).

Acknowledgements

This work was supported by the National Natural Science Foundation of China (grant number **51864021**), and the authors are grateful for the helpful suggestions and evaluations given by many anonymous reviewers.

Author contributions

Yunnan Chen wrote the main manuscript text, Jaili Xu and Yuting Li were responsible for conceptualization, formal analysis, investigation, methodological examination, etc.

Declarations

Competing interests
The authors declare no competing interests.

Additional information
Supplementary Information The online version contains supplementary material available at https://doi.org/10.1038/s41598-024-74115-y.

Correspondence and requests for materials should be addressed to Y.C.

Reprints and permissions information is available at www.nature.com/reprints.

Publisher's note Springer Nature remains neutral with regard to jurisdictional claims in published maps and institutional affiliations.